Contrib Mineral Petrol (2004) 147: 48–57
DOI 10.1007/s00410-003-0539-x

ORIGINAL PAPER

C. Lemaire · S. C. Kohn · R. A. Brooker

The effect of silica activity on the incorporation mechanisms of water in synthetic forsterite: a polarised infrared spectroscopic study

Received: 13 March 2003 / Accepted: 27 October 2003 / Published online: 20 January 2004

Abstract Pure forsterite crystals were grown from hydrous melts using controlled cooling experiments at 2.0 GPa and varying the bulk Mg/Si ratio from 2.0 to 1.5. Oriented single crystals were then studied by polarised infrared spectroscopy. The spectra of the samples with the lowest silica activity ($a\mathrm{SiO_2}$) contain the main OH bands in the range 3,620–3,450 $\mathrm{cm^{-1}}$ only. In contrast, the spectra of the samples synthesised with the highest $a\mathrm{SiO_2}$ contain additional pleochroic bands at 3,160, 3,220 and 3,600 $\mathrm{cm^{-1}}$. The variations are interpreted in terms of protonated silicon vacancies being dominant at low $a\mathrm{SiO_2}$ and Mg vacancies dominant at high $a\mathrm{SiO_2}$. Xenolithic mantle olivines generally do not have the spectrum expected for orthopyroxene buffered conditions, suggesting that they re-equilibrated with their host melts during ascent, but mantle olivine from the Zabargad peridotite massif probably is in equilibrium with the coexisting orthopyroxene.

Introduction

The physical and chemical properties of the Earth's mantle are the dominant control on the most important large scale processes which have prevailed during the evolution of the Earth. These include plate tectonics, formation of the crust, and degassing of the oceans and atmosphere. Compared with other trace elements, small amounts of water can have a disproportionately large effect on the properties of the mantle, so knowledge of its concentration, distribution and incorporation mechanisms is crucial for understanding global geodynamics. The importance of water in the mantle has been recognised for many years; its effect on increasing the degree of melting at a given temperature (e.g., Hirose and Kawamoto 1995) and decreasing mantle viscosity (e.g., Hirth and Kohlstedt 1996) are well documented and it has been suggested that water influences seismic velocities and anisotropy (Karato and Jung 1998; Jung and Karato 2001) and electrical conductivity (Karato 1990). Such data are now being used to constrain the way water is stored, transported and distributed between the exosphere and the mantle (e.g., Franck and Bounama 1995; Richard et al. 2002).

To elucidate the role of water in large scale mantle processes, the interaction between protons and point-defects in nominally anhydrous minerals (NAMs) must be understood. Such interaction has implications for both the sites occupied by H in the structure and the solubility of H in NAMs in the Earth's mantle (e.g. Bell and Rossman 1992; Ingrin and Skogby 2000). Olivine is the most abundant mineral in the upper mantle, so an understanding of the mechanisms of incorporation of water in this phase is a priority.

Infrared spectroscopy is a very useful probe of OH in NAMs such as olivine because of its high sensitivity. The stretching frequencies provide information on the chemical environments of the OH groups, and OH orientations can be deduced using polarised measurements. Although many workers have reported infrared spectra for natural olivine, the OH stretching spectrum is very variable and poorly understood. Samples commonly contain a large number of bands in the range 3,400 to 3,650 $\mathrm{cm^{-1}}$ but frequencies as low as 3,200 $\mathrm{cm^{-1}}$ have been seen in some samples. The variation could be related to differences in silica activity, oxygen fugacity and iron oxidation state or water fugacity, or could be related to the trace element concentrations of different samples.

There are major disagreements between the previously published experimental studies of the solubility and dissolution mechanisms of water in olivine. For

Editorial responsibility: T.L. Grove

C. Lemaire · S. C. Kohn (✉) · R. A. Brooker
Department of Earth Sciences,
University of Bristol, Queens Rd., Bristol, BS8 1RJ, UK
E-mail: simon.kohn@bristol.ac.uk
Tel.: +0044-117-3315002
Fax: +0044-117-9253385

example, Kohlstedt et al. (1996) and Bai and Kohlstedt (1992, 1993) observed that for experiments under orthopyroxene-buffered conditions, the main peaks are at 3,450–3,650 cm^{-1}. In contrast, Matveev et al. (2001) suggested that under these conditions, peaks at 3,300–3,400 cm^{-1} are dominant and the 3,450–3,650 cm^{-1} peaks are absent.

In order to address one aspect of this complex problem, the approach of the present study is to simplify the system, and determine the water dissolution mechanism in high purity Mg_2SiO_4 forsterite under a range of SiO_2 buffering conditions. This approach removes some of the variables related to the presence of iron and trace elements, in particular the role of oxidation state. We show that large changes in the mechanism of hydroxyl incorporation occur as a function of silica activity in the synthesis environment. These are interpreted in terms of protonated Si or Mg vacancies in the crystals.

Synthesis and analysis of crystals of forsterite

Starting material and HP/HT synthesis

Forsterite crystals were synthesized from a mixed powder of high purity $Mg(OH)_2$ (supplied by Intermag Co. Ltd.) and specpure SiO_2 (Aldrich). The mixtures had Mg/Si ratios of 2, 1.85 and 1.5 (Table 1), giving bulk water concentrations in the range 20 to 18 wt%. For each experiment, the powder was ground in an agate mortar and loaded into a Pt capsule of 6 mm diameter and 14 mm length. The sealed capsule was surrounded by an alumina sleeve within a talc-Pyrex pressure cell. A tapered graphite furnace was used, so that the thermal gradient is small, with a temperature variation of less than 20 °C along the capsule and the temperature was monitored using a type D, W-Re thermocouple. The experiments were performed at 2.0 GPa in an end-loaded piston-cylinder apparatus. All the samples, except Fo#1, were heated above the liquidus at 1,550 °C for 1 h, then cooled over a period of a few minutes to 1,470 °C, which is a few tens of degrees above the estimated water saturated forsterite liquidus (Kushiro and Yoder 1969). To confirm that no olivine crystallisation occurs above 1,470 °C, one experiment was quenched immediately after cooling from 1,550 to 1,470 °C and, as expected, subsequent examination showed that it contained only a quench phase. After the initial cooling to 1,470 °C, the samples were then subjected to a controlled cooling ramp, with cooling rates of 800 °C/h or 1 °C/h. The final temperature is 1,400 °C when the cooling rate was 1°/h and 1,250 °C when the cooling rate was 800°/h. The fast cooled samples were held at 1,250 °C overnight before quenching. Fo#1 had a somewhat different temperature history; the temperature was reduced manually in a series of steps from 1,480–1,250 °C. After the experiments, the capsules were pierced and in all cases excess water was released. The crystals of forsterite obtained using this method were typically tabular in habit, with dimensions on the order of 1 mm.

Transmission electron microscopy

Transmission electron microscopy (TEM) was used to examine crystals from two of the experiments (Fo#1 and Fo#6) to ensure that the crystals of forsterite are free of any submicroscopic inclusions of any other phases. The observations were carried out on a Philips EM430 by Dr. Roger Vincent in the Department of Physics of the University of Bristol (UK). The microscope accelerating voltage was 250 kV. Samples were prepared by crushing the crystals gently, followed by deposition of the fragments onto a 200 mesh Cu grid. Many of the fractured edges were electron transparent. The observed areas did not reveal any phases other than forsterite. This was confirmed by analysis of diffraction patterns acquired from both crystals. To check the homogeneity of the crystals with nanometre resolution, we observed several edges at a magnification of 100,000. Using the bend contour and thickness fringe contrast near the Bragg condition, the areas revealed a very clear and uniform structure, except for some dislocations at the extremities, which might be intrinsic to the crystals or may have been induced by crushing. No planar defects of clinohumite or serpentine were observed (cf. Kitamura et al. 1987), furthermore no signal of such phases were detected by micro-infrared (see below). The fact that we did not observe any submicroscopic phases is further evidence that our crystals of forsterite are pure. Although the transparent areas were micron-sized, and therefore only

Table 1 Experimental conditions of synthesis and water content of forsterite. All the experiments are performed at 2.0 GPa

Sample	MgO/SiO_2 (mol. ratio)	H_2O (wt.%)	T°C range	Duration of dwell	Cooling (°C/hour)	C_{H2O} (ppm)[c]	C_{OH} ($H/10^6Si$)
Fo#1	2	20.3	1,480–1,250	12 h	800[b]	750 ± 100 (6)	12,200 ± 1,600
Fo#2	2	20.3	1,470–1,430	None	1	100 ± 10 (3)	1,625 ± 160
Fo#3	2	20.3	1,470–1,250	12 h	800	60 ± 15 (3)	1,000 ± 250
Fo#4	1.85	19.8	1,470–1,400	None	1	110 ± 10 (3)	1,800 ± 160
Fo#5[a]	1.85	19.8	1,470–1,250	12 h	800	42 ± 5 (3)	680 ± 80
Fo#6	1.5	18.3	1,400–1,275	12 h	1	70 ± 20 (6)	1,130 ± 325

[a]Enstatite crystals were also found in the capsule
[b]Approximate, because the cooling was carried out manually in a series of steps
[c]The concentrations (in wt ppm) have been calculated from the polarised IR spectra on several crystals for each sample; the number of which is indicated in parentheses

included a small part of the crystal, the TEM results are consistent with observations of the crystals by optical and scanning electron microscopy.

FTIR spectroscopy

Infrared spectra were measured using a microscope attached to a Nicolet 800 Fourier transform infrared spectrometer operating between 6,000 and 650 cm^{-1}. A KBr beamsplitter and MCT detector were used to collect 256 scans at a resolution of 4 cm^{-1} and polarisation of the electric vector was produced by a ZnSe polariser. The microscope was enclosed within a box that was purged with high purity nitrogen to reduce fluctuations in the atmospheric H_2O and CO_2. The analyses were carried out through a 100 μm diameter spot.

The clearest crystals free of cracks and bubbles, were chosen for the FTIR analyses. The samples were doubly polished on two or three orthogonal directions. The orientation of sample Fo#4 was checked with a face indexing procedure by single-crystal X-ray diffraction. As the maximum absorption is observed along the three crystallographic axes (e.g., Libowitzky and Rossman 1996), polarised spectra were recorded with the electric vector parallel to these three directions (x, y and z in the Pbnm space group). The IR bands in the range of the silicate overtone vibrations (1,200–2,200 cm^{-1}), are strongly dependent on orientation (Fig. 1a). These peaks were therefore used to determine the orientations of the other samples (which were not indexed using XRD). Note that the allocation of the overtone bands in the unpolarised measurements reported by Jamtveit et al. (2001) is not consistent with the Pbnm space group used here.

The water content was determined using the Beer-Lambert law and the calibration of the integrated molar absorption coefficient by Libowitzky and Rossman (1997). The density was chosen as 3.27 $g.cm^{-3}$ and the thickness was measured by a digital travel gauge. The integrated absorbance was obtained by fitting the spectra between 3,000 and 3,800 cm^{-1} using Igor Pro and the water content of each sample was obtained by summing the data for all three directions.

With the exception of experiment Fo#6, the spectra for crystals from a given experiment (3–6 for each sample) are very similar. Sample Fo#6, however, is very heterogeneous from the top to the bottom of the capsule, and spectra for five different crystals are presented here.

Results

The IR spectra of crystals of forsterite show strong, well resolved, vibrational features characteristic to each crystallographic axis. As an example, Fig. 1b shows the polarised IR absorption in the OH stretching range of Fo#1. This is the sample containing the highest concentration of water (750 wt ppm, Table 1), and as a result, the IR absorption bands are easily observed above the noise. All the OH bands of this sample are at high frequency, in the range 3,450–3,620 cm^{-1}, and are strongly pleochroic. The main bands are at 3,613, 3,580 and 3,566 cm^{-1}, and in addition there is a group of smaller bands between 3,530 and 3,555 cm^{-1} and a well-resolved band at 3,480 cm^{-1}. Polarised spectra for all the samples are shown in Fig. 2. Spectra for several crystals of Fo#6 are included as this sample was heterogeneous (see above). Additional bands are observed, compared with Fo#1, particularly in the samples with $Mg/Si < 2$. A summary of the positions, pleochroism and approximate relative intensities is given in Table 2. Two of the three main additional bands (3,220 and 3,160 cm^{-1}) have a maximum absorption when the electric vector is parallel to z, and the third (3,600 cm^{-1}) has a maximum absorption when it is parallel to y.

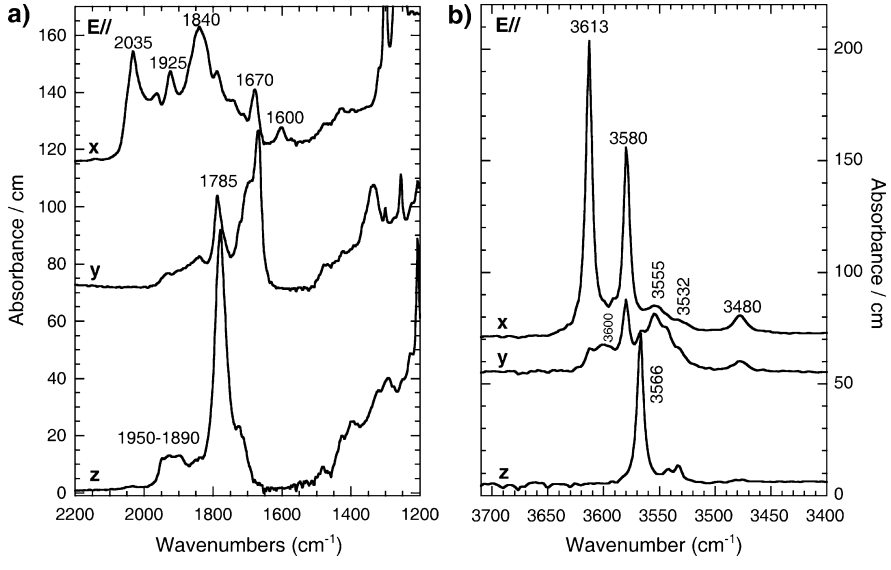

Fig. 1 Polarised and oriented FTIR spectra of Fo#1 with E // to x, y and z (**a**) Si-O overtones in the crystallographic directions used for orienting crystals. (**b**) OH stretching modes. No OH stretching bands are observed below 3,400 cm^{-1} in this sample

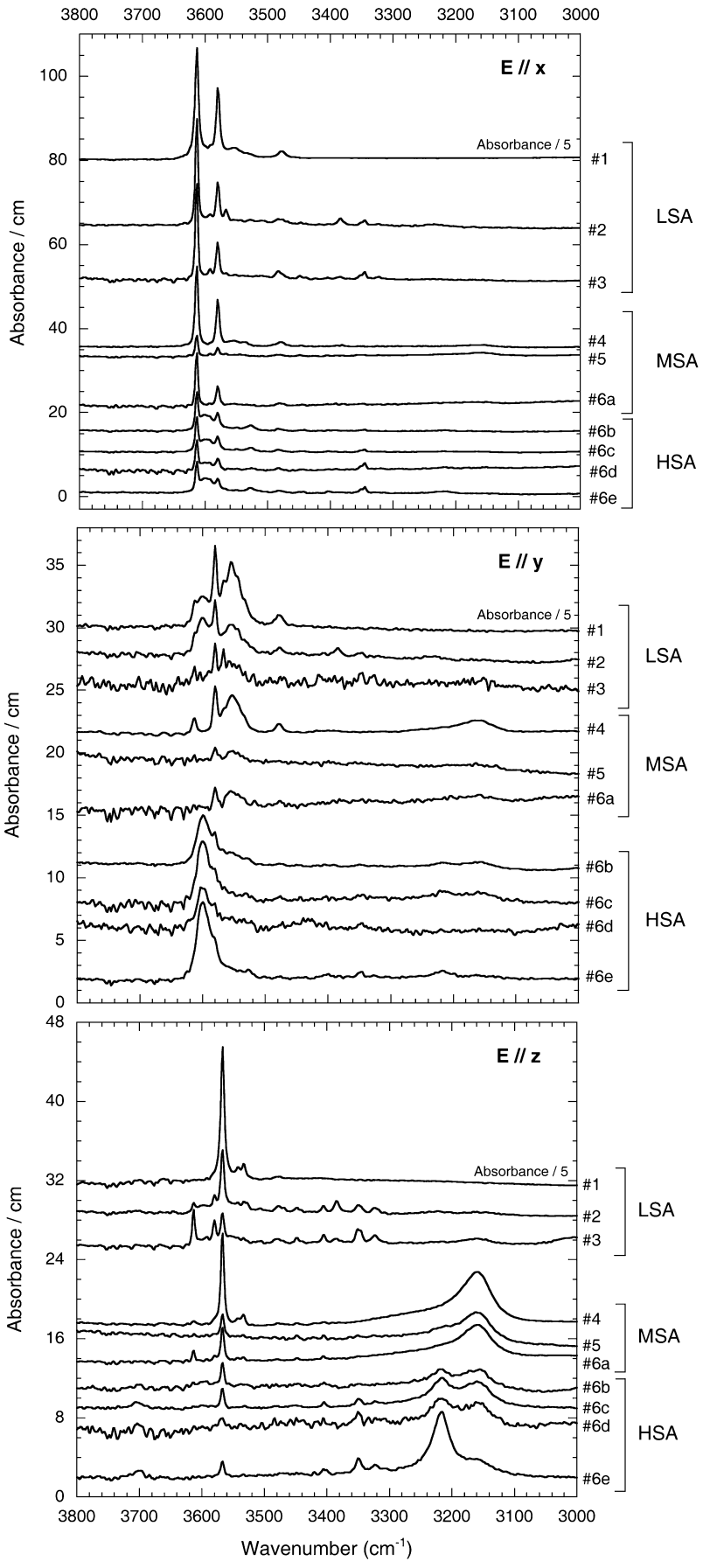

Fig. 2 Polarised OH stretching spectra with the electric vector parallel to x, y and z directions of all the samples. The spectra are stacked in order of apparent $a\mathrm{SiO_2}$ increasing down the figure. *LSA*, *MSA* and *HSA* are low, medium and high silica activity, respectively

Table 2 Features of all OH stretching vibrational bands

ν (± 2 cm^{-1})	Maximum intensity[a]	Pleochroism	Present in samples	OH point defects[b]
3,613	High	x > > y	LSA—MSA—HSA	V_{Si}
3,600	High	y≥x	HSA	V_{M2}
3,580	High	x > y	LSA—MSA—HSA	V_{Si}
3,566	High	z > > y	LSA—MSA—HSA	V_{Si}
3,555	High	y > > x	LSA—MSA	V_{Si}
3,542	Low	y > > z	LSA—MSA	
3,535	Low	y	LSA—MSA	
3,527	Low	x	HSA	
3,480	Low	x > > y > > z	LSA—MSA	
3,402	Low	z > x≈y	LSA—HSA	
3,385	Low	x = z > y	LSA	
3,348	Low	z > x > y	LSA—HSA	
3,325	Low	z	LSA—HSA	
3,220	High	z	HSA	V_{M2}
3,160	High	z	MSA	V_{M1}
3,700[c]	Low	z	HSA	

[a]The relative maximum intensity found in any of the experiments
[b]The speculated location of H related to the major OH vibrational bands
[c]The origin of this band is uncertain and may be due to the presence of serpentine

As the only significant compositional variable in our experiments is the Mg/Si ratio, the samples will be classified on this basis. The spectra for Fo#2 and Fo#3 are broadly similar to the spectra for Fo#1, and this group of three samples will be referred to as the low silica activity (LSA) samples. Fo#4, Fo#5 and Fo#6a are similar to each other and will be referred to as the medium silica activity (MSA) samples, and finally Fo#6b-Fo#6e which are substantially different from all the other samples will be referred to as the high silica activity (HSA) samples.

In the sample Fo#6 (Mg/Si ratio in the starting material of 1.5), IR spectra of five crystals are presented because of major variations of the spectra. Fo#6a is one of the extremes (its IR features are similar to the Mg/Si = 1.85 samples) and Fo#6e is the other. The spectra of Fo#6b–d are intermediate between these two end-members. There is a correlation between the apparent silica activity and the position of the crystals inside the capsule. Fo#6a was located at the top of the capsule and Fo#6e at the bottom, whereas the others were in the middle. The temperature gradient inside the capsule is about 20 °C at 1,400 °C. Consequently, with a cooling rate of 1 °C/h, the top part starts to crystallise 20 h before the middle. From initiation of crystallisation, the Mg/Si ratio in the remaining aqueous fluid decreases continuously: at 10% of crystallisation, Mg/Si ratio is equal to 1.46 and at 50% of crystallisation, it is equal to 1.2. Thus, Fo#6a probably crystallised from Mg/Si ratio of 1.5 and Fo#6e from the Mg depleted liquid. This could explain the major differences between the crystals in this experiment. It is interesting to note that holding the capsule for 12 h at a final temperature of 1,275 °C and 2.0 GPa does not homogenise the sample and overprint these differences.

The water concentrations in the samples appear to vary with cooling rate; with the exception of Fo#1 (which had a complex and less well constrained cooling rate), the rapidly grown crystals contain a lower concentration of H in their structure. However the final temperature is also lower for the rapidly cooled samples

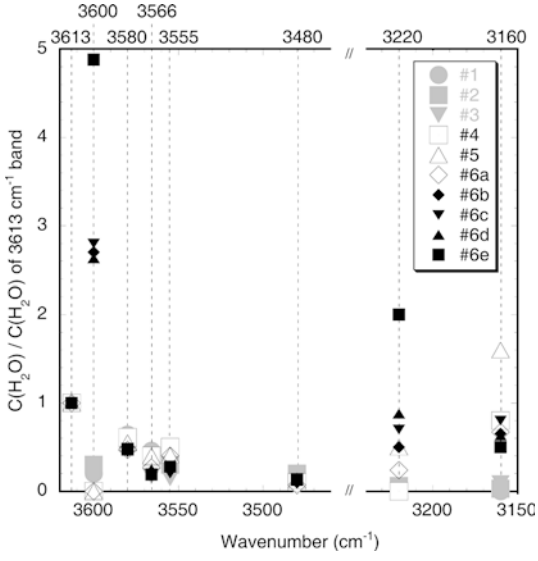

Fig. 3 The concentration of water, $C(H_2O)$, corresponding to each of the main peaks, normalised to $C(H_2O)$ corresponding to the 3,613 cm^{-1} band. Note that the ratio for some peaks is approximately constant, whereas others show large variations from sample to sample

(see Table 1). It is notable that the point-defect structure of the samples, does not vary with cooling rate or total water concentration as no significant difference is observed between the spectra of Fo#2 and Fo#3 or between Fo#4 and Fo#5 in Fig. 2.

As there are clearly a large number of bands, showing complex changes as a function of silica activity it is important to identify any significant correlations between them. Figure 3 shows the OH concentration corresponding to each of the main bands normalised to the 3,613 cm^{-1} band. Some bands such as those at 3,600, 3,220 and 3,160 cm^{-1} show large variation, whereas others are approximately constant. The peaks at 3,613, 3,580, 3,566, 3,555 and 3,480 cm^{-1} can be considered to behave as a group, and perhaps have a similar point defect origin. Similarly, the peaks at 3,600 and

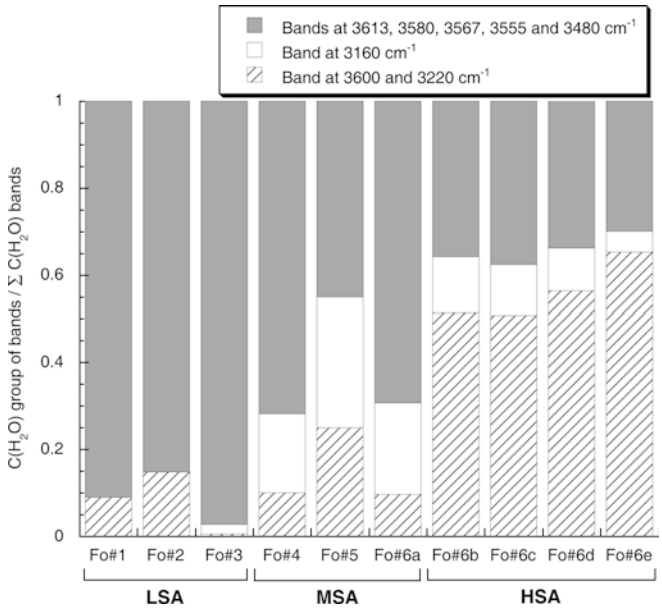

Fig. 4 Sample to sample variation in the relative concentration of water in the three groups of OH stretching bands

3,220 cm^{-1} behave as a pair, being most significant in the HSA samples. The peak at 3,160 cm^{-1} is not related to any of the other peaks, as it shows a maximum intensity in the MSA samples. These features are summarised in Fig. 4, where the relative proportions of water in each of the three groups are illustrated.

Discussion

Mechanisms of H incorporation

As shown in Fig. 4, the incorporation mechanism of protons in forsterite is strongly correlated with $aSiO_2$, with the peaks at 3,613, 3,580, 3,566, 3,555 and 3,480 cm^{-1} being dominant at low $aSiO_2$ and peaks at 3,160, 3,600 and 3,220 cm^{-1}, being dominant at higher $aSiO_2$. Changes in olivine spectra as a function of $aSiO_2$ were also observed by Matveev et al. (2001) for a natural iron bearing system. They found that different bands were observed depending on whether the natural olivine was buffered at low or high silica activity. The spectra of olivine buffered with the magnesiowüstite contain only high frequency bands and are similar to Fo#1, #2 and #3, whereas olivine buffered with orthopyroxene has a different set of bands in the range 3,285–3,380 cm^{-1}. This major change was explained by the variations of the silica activity in the environment and although the high silica activity bands are in a different position, there are clearly some similarities with the observations of this study. As the Matveev et al (2001) experiments were on natural, Fe-bearing samples, the 3,285–3,380 cm^{-1} peaks may be related to the role of the oxidation state of iron or the presence of other trace elements.

In Kohlstedt et al. (1996), the low end of the pressure range of the study is comparable with this study, and the spectra are also polarised, enabling a direct comparison to be made. Despite the difference in composition (natural olivine vs. specpure forsterite), major peaks at 3,613, 3,580 and 3,567 cm^{-1} and other smaller bands between 3,530 and 3,550 cm^{-1} are present in both studies. However, the lower frequency bands observed here were not reported by Kohlstedt et al (1996). The similarities in the spectra (despite the different silica activity conditions of the experiments) are not yet understood and further work is required to explain the apparently contradictory results of the different studies.

In the present study, all the synthesised crystals are Fe-free forsterite, so the incorporation of hydrogen cannot involve oxidation/reduction of iron. The alternative possibilities for protons to enter the structure are by compensating the charge defects in vacancies, Si^{4+} in the tetrahedral site or Mg^{2+} in the distinct octahedral sites M1 and M2, or as hydrogen interstitials (e.g., Libowitzky and Beran 1995; Bai and Kohlstedt 1993). For the fully protonated vacancies, the hydroxyl defects associated are then $(4H)^{x}_{Si}$ or $(2H)^{x}_{Mg}$, and for the interstitial one $H^{\bullet}$ (according to the Kröger-Vink defect notation). In this schema, the relationship between H incorporation and silica activity is as follow. The lower the $aSiO_2$ the more the silicon vacancies in tetrahedra will be favoured whilst for higher $aSiO_2$, more magnesium vacancies in octahedra will be favoured. A model for OH incorporation can therefore be constructed by combining the constraints of the $aSiO_2$ dependence with the observed pleochroism of the bands.

The OH bands at 3,613, 3,580, 3,566, 3,555 and 3,480 cm^{-1} are assigned to H compensating Si vacancies. At first sight the three largest and narrowest bands can be correlated with specific positions in the structure (Fig. 5a). For example, the 3,566 cm^{-1} peak can be attributed to H located along the O3-O3 edge of the tetrahedron and thus orientated along z. Similarly, the 3,613 and 3,580 cm^{-1} bands which have maximum intensity along x, can be attributed to H located along the O1-V_{Si} and O2-O1 joins, respectively. However, it is not possible to assign all the OH bands in this way. This is possibly because of interactions between OH vibrations for clusters of OH, because of distortions in the shape and size of the tetrahedron away from the ideal Si-occupied tetrahedron in forsterite or because of the flexibility in the conformations of clusters.

The proposed mechanism involving protonated Si vacancies is consistent with the theoretical studies of Brodholt and Refson (2000) and Braithwaite et al. (2003) which showed that Si vacancies are far more energetically favourable in presence of protons than in dry samples. The observed orientations and the frequency differences between the bands is somewhat similar to the predictions of Braithwaite et al. (2003) for the hydrogarnet defect. In both the theoretical study and our experimental data, the highest frequency band is oriented along x, there is a band 30 cm^{-1} lower in

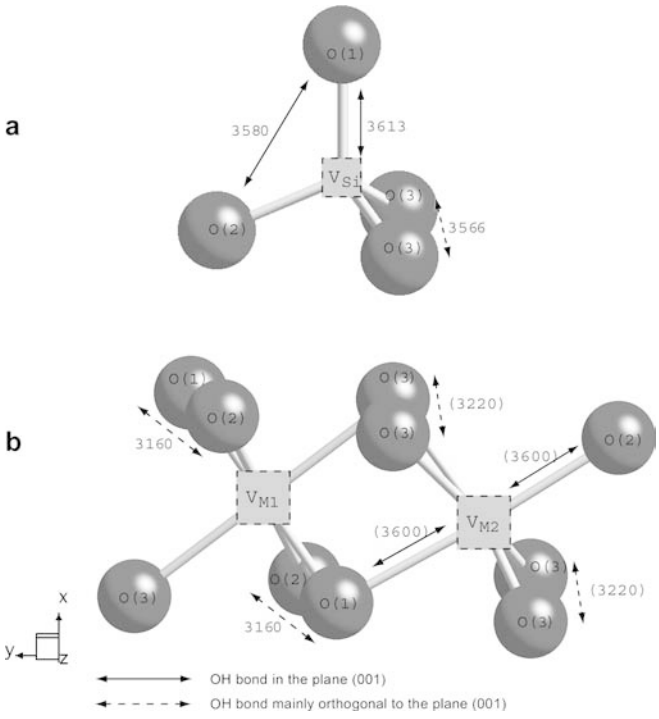

Fig. 5 The structure of forsterite with possible locations of OH, as indicated by the directions of the arrows. The related OH frequency is specified. (a) One example of a configuration involving a Si vacancy (b) M1 and M2 vacancies. The two M-sites are illustrated together to show the geometric relationship between them, but it is not implied that adjacent M1 and M2 sites can both be vacant

frequency along x and there is a band 55–60 cm^{-1} lower along y. It should be noted that the IR stretching frequencies which we attribute to H related to Si vacancies, are close to the frequency observed for hydrogarnet substitution in silicate garnets (around 3,600 cm^{-1}) (e.g., Rossman and Aines 1991). These frequencies would not be predicted by the correlation of Libowitzky (1999) unless the O-O distances in an SiO_4^{4-} tetrahedron are increased substantially upon creation of the vacancy.

Other aspects of the data agree less closely with this hypothesis. A complication in the experimental data is that there are at least 5 rather than 4 bands of significant intensity, with the same $a SiO_2$ dependence. It could be argued that this results from the presence of V_{Si} with a range of numbers of protons or different configurations of the protons within the hydrogarnet species. We consider the latter more likely as it maintains local charge balance.

The three bands at 3,600, 3,220 and 3,160 cm^{-1} are enhanced in the samples with higher silica activity, therefore they are attributed to OH associated with Mg vacancies. As these IR bands are pleochroic, (with maximum absorption along z), the corresponding OH bonds must be related to a well-defined point-defect and cannot arise from randomly oriented interstitial OH. The band at 3,160 cm^{-1} has a maximum intensity in the MSA samples and the 3,600 and 3,220 cm^{-1} bands increase together in the samples with highest silica activity (Figs. 3 and 4). The fact that the intensities of all three bands do not increase in parallel with each other suggests that the 3,160 cm^{-1} band is related to one type of Mg vacancy and the 3,600 and 3,220 cm^{-1} bands are related to another. We suggest that the 3,160 cm^{-1} band is related to M1 vacancies and 3,600 and 3,220 cm^{-1} bands are related to M2 vacancies (Fig. 5b) for the following reasons:

– M1 has a centre of symmetry, so pairs of OH close to opposite edges of the octahedron would be identical and therefore give rise to a single band. We propose that the H is located along the O2-O1 vector in M1, matching the OH orientation observed in FTIR (along z). Theoretical studies (Brodholt and Refson 2000; Braithwaite et al. 2003) have previously suggested that protonation at O2, charge-balanced by an M1 vacancy, is a stable configuration consistent with our assignment.
– M2 is a much more distorted site, producing non-identical pairs of OH. Thus the two H required to charge-balance an Mg vacancy would give two distinct infrared stretching bands, as observed. To be more specific about the location for the two protons in the M2 site, the orientation and frequency must be accounted for. One potential location is on either O1 or O2 atoms, pointing along y towards the centre of the vacancy. This would be consistent with the relatively high frequency of 3,600 cm^{-1}. The other most probable position is on one of the O3-O3 edges which lie along z. It should be noted that there is also a 3,600 cm^{-1} band in Fo#1 and Fo#2, however, we believe that this band has a different origin from the 3,600 cm^{-1} band in the HSA samples because the pleochroism is somewhat different, being more strongly oriented along y.

We do not favour the alternative hypothesis that all of the three HSA bands are related to M1, because there is no clear reason why a rearrangement of H within the M1 octahedron would occur at some specific silica activity. Although we do not have a definitive explanation for the change from M1 to M2 vacancies, the following scenario is a possibility: The first Mg sites to become vacant as $a SiO_2$ is increased are M1 sites, as M1 vacancies have a lower energy than M2 vacancies (Brodholt 1997). These become protonated giving the 3,160 cm^{-1} band. As $a SiO_2$ is increased further, M2 vacancies start to have a significant abundance. If the energy of protonated M2 vacancy is lower than the energy of a protonated M1 vacancy (we note that there is no information to support or refute this possibility as the calculations were performed in dry conditions), then the balance of OH within the forsterite will switch, with the proposed M2 vacancy hydroxyl at 3,600 and 3,220 cm^{-1} becoming the most abundant.

The observed frequencies of 3,220 and 3,160 cm^{-1} are surprisingly low. According to the correlation of Libowitzky (1999), such frequencies imply short O-H···O distances, yet O-O distances in cation-occupied

octahedra are longer than O-O distances in Si tetrahedra. This observation can be explained in part by changes in the size and shape of the sites induced by cation vacancies and protonation. Another contribution is the effect of the covalent bonds around the protonated oxygen atoms. In the case of a silicon vacancy, the oxygens are bonded to 3 Mg and in the case of the Mg vacancy, the oxygens are bonded to 2 Mg and 1 Si. This change of covalency could have a major effect on the related O-H strength. Indeed, the stronger Si-O bond compared to Mg-O would induce a weaker O-H bond. Further support for the assignment is provided by the results of Braithwaite et al. (2003), who calculated that $(2H)^{x}_{Mg}$ have lower IR frequencies than those of $(4H)^{x}_{Si}$.

Although the main goal of this paper was not to determine the solubility of hydrogen in olivine, we note that the slowly-cooled samples (which probably represent the closest approach to equilibrium) contain about 100 wt ppm H_2O. This value is comparable with extrapolation of the Kohlstedt et al. (1996) data to 2.0 GPa despite differences in composition, temperature and the fact that in the present study the crystals were grown during the runs. The similarity in both the frequencies of the IR bands and the dissolved water concentration between the data of Kohlstedt et al. (1996) and this study suggests that for the high dissolved water concentrations in these experiments, the role of Fe in the incorporation mechanism may be less important than previously suggested (e.g., Mackwell and Kohlstedt 1990; Bai and Kohlstedt 1993; Kohlstedt et al. 1996). The very high (presumably disequilibrium) solubility in Fo#1 is probably related to a very high growth rate. High growth rates could lead to a very defective crystal, which could then soak up H to charge balance Si vacancies. The re-equilibration of such oversaturated crystals would be slow because it would involve diffusion of Si vacancies through mm-sized crystals. This explanation for the high H_2O concentration in Fo#1 could also apply to the high concentration of water in synthetic forsterite observed by Kohn (1996), where crystals were grown by recrystallisation of a dry forsterite powder.

Implications to natural mantle olivine

Natural mantle olivine samples show a great diversity of OH stretching spectra (e.g., Miller et al. 1987). This diversity could reflect chemical inhomogeneity in the mantle, or could be due to changes in the amount and location of OH in the olivine structures during transport of mantle samples to the surface. Many of the peaks observed for our samples synthesised in the simple MgO-SiO_2-H_2O system are also observed in natural mantle olivine crystals (see Fig. 6 and data in Miller et al. 1987), so our experimental data may be able to shed some light on this problem.

Most reported mantle olivine spectra are dominated by peaks in the range 3,450–3,650 cm^{-1}. A sample from the Thumb, Colorado Plateau, USA, is typical and its spectrum is included in Fig. 6. The surprising feature of this type of olivine spectrum is that experimental data (Matveev et al. 2001 and this study) suggest that these high frequency bands represent low $a SiO_2$ conditions, and are not consistent with the presence of coexisting orthopyroxene. One explanation is that the majority of xenolithic olivines have completely re-equilibrated with the magma that transports them to the surface. This is often a melt such as an alkali basalt or kimberlite with a low silica activity.

One possible exception is the xenolith from Monastery Farm, South Africa (Miller et al. 1987) which shows additional peaks at 3,613 cm^{-1} and at lower frequencies, in particular 3,230 cm^{-1}. Both the 3,613 and 3,230 cm^{-1} peaks have the same pleochroism as the analogous peaks in our experimental samples. The

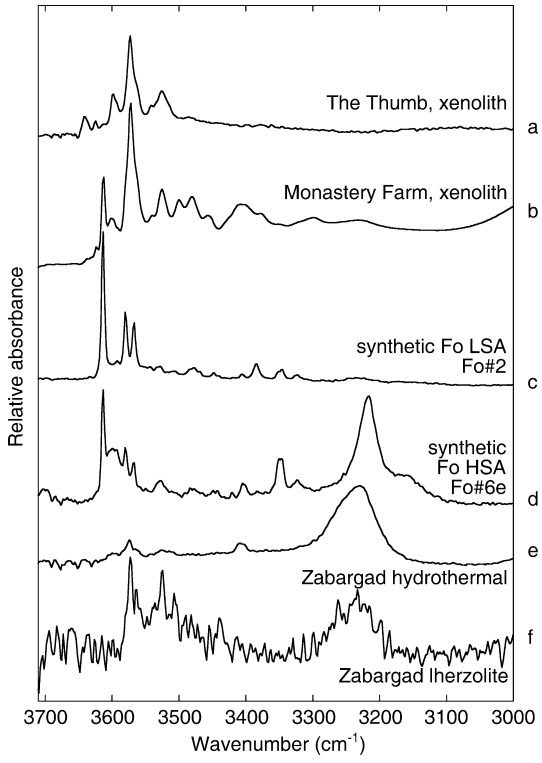

Fig. 6 Spectra of various natural olivine samples compared with synthetic samples from this study. The top spectrum is unpolarised, the spectra for the other samples are the sum of the polarised spectra taken for the x and z directions. (*a*) is typical of many mantle xenoliths. It is an unpublished spectrum from a garnet lherzolite xenolith, transported by a minette lava (The Thumb, Colorado Plateau, USA). (*b*) is a mantle xenolith transported by a kimberlite, (Monastery Farm, South Africa, in Miller et al. 1987). (*c*) and (*d*) spectra are samples from this study. (*e*) and (*f*) are unpublished spectra of olivine samples from Zabargad, Egypt (collected by RA Brooker). The hydrothermal sample is similar to previously published spectra on gem quality Zabargad olivines (e.g., Beran and Putnis 1983; Miller et al. 1987) but the relative intensity of the 3,230 cm^{-1} band compared to the higher frequency peaks is highly variable from crystal to crystal (as are water contents). The lherzolite Zabargad olivine has not previously been studied by IR, and other crystals examined from the same hand specimen (all in contact with opx) are all similar to the one shown

presence of a peak at 3,230 cm^{-1} is consistent with high $aSiO_2$ conditions and implies that the dissolution mechanism we have observed in high purity forsterite can also occur in natural Fe-bearing samples. A peak at about 3,230 cm^{-1} has also been seen in olivine phenocrysts from an Icelandic picrite (Jamtveit et al. 2001). In contrast, we know of no examples of natural olivines with a peak at 3,160 cm^{-1}; if our interpretation of this peak in terms of M1 vacancies is correct, its absence in natural samples may be related to an interplay between the ordering of Fe^{2+} onto M2 sites at high temperature (e.g., Redfern et al. 2000) and the energetics of Mg and Fe vacancy formation. However, the influence of water on the partitioning of Fe between M1 and M2 octahedral sites is not known. Another unusual feature of the Monastery Farm sample is that it has an exceptionally high water concentration. It is possible that both the presence of additional peaks and the high total dissolved water concentration result from rapid quenching during eruption in a kimberlite magma. Thus, it is conceivable that the 3,613 and 3,230 cm^{-1} peaks are present in other mantle olivines in situ, but that water is preferentially lost from these sites during ascent.

Two different types of olivine from Zabargad Island in the Red Sea provide an interesting contrast to the xenolith samples. The famous hydrothermal, cm-sized, gem-quality olivines are found as terminated prisms growing into free cavities in a serpentinite matrix. The composition is Fo90 with a high and variable NiO content (0.35–0.8 wt%), in some cases along the length of a crystal. According to Sciuto and Ottonello (1995) these precipitated at a thermal maximum (500 °C at 0.1 GPa) after dissolution of serpentine previously derived from lower temperature interaction between heated seawater and mantle peridotite. If this is correct then the bulk Mg/Si ratio of the system is 1.5, similar to our HSA experiments. The spectrum for the hydrothermal olivine (Fig. 6, see also Beran and Putnis 1983; Freund and Oberheuser 1986; Miller et al. 1987) does indeed contain a large peak at 3,230 cm^{-1}, very close to the peak observed in Fo#6e, and with the same pleochroism, strongly suggesting that a very similar defect is responsible. The other olivine sample shown in Fig. 6 is from the original and unaltered pristine mantle peridotite that has been tectonically emplaced on Zabargad. Even though the paragenesis is very different from the hydrothermal olivine, this sample also shows the band at 3,230 cm^{-1} suggesting a high $aSiO_2$, consistent with the coexisting opx. Other examples of non-xenolithic mantle olivine are difficult to find in the literature, as peridotitic massifs are usually subjected to pervasive alteration during emplacement and subsequent exposure in climates less arid than Zabargad. It remains to be seen whether the differences between the Zabargad tectonically emplaced olivine and xenolithic olivines are providing fundamental information about the problems of sampling the mantle via xenoliths.

Conclusions

The experimental work reported here has shown that the polarised IR absorption signal of OH-bearing forsterite depends strongly on the silica activity during synthesis. For the low silica activity samples, the bands are mainly at high frequencies (3,613, 3,580, 3,566, 3,555 and 3,480 cm^{-1}). In our experiments, these bands remain even at high silica activity but their relative intensities decrease compared with lower frequency bands. For our medium silica activity samples, the main feature is one broad band at 3,160 cm^{-1} (when the electric vector E vibrates parallel to z). For our highest silica activity samples, two new large bands are observed at 3,220 cm^{-1} (E//z) and 3,600 cm^{-1} (E//y). The definition of group I (3,450–3,800 cm^{-1}) and group II (3,000–3,450 cm^{-1}) bands (Bai Kohlstedt 1993) for different H defects is therefore inadequate in the light of these new results.

The bands at high frequency [3,450–3,620 cm^{-1}] (excluding the 3,600 cm^{-1} band) are attributed to OH groups associated with Si vacancies. The bands at 3,160, 3,220 and 3,600 cm^{-1} are observed in crystals synthesised at the highest silica activity and are thus assigned to OH groups associated with M-site vacancies.

Few natural samples of mantle xenolithic olivine seem to have the orthopyroxene buffered features. This may be because of interaction of the xenoliths with their host melts during their ascent from the upper mantle, or because of partial melting along grain boundaries resulting from decompression or heating. In the case of one previously published Monastery Farm xenolithic olivine, such effects may be limited by fast ascent. Mantle olivine from Zabargad (which is uplifted tectonically rather than being carried by a melt) shows features similar to orthopyroxene buffered conditions and, together with the Monastery Farm sample, may be the most representative of mantle olivine.

Acknowledgements This work has been enabled with the financial support of the EU Research Training Network "Hydrospec" (contract No. HPRN-CT-2000-00056). We are grateful to Dr. Yann Morizet for help with the piston-cylinder experiments, Dr. Jonathan Charmant (Department of Chemistry, University of Bristol) for performing single crystal X-ray diffraction measurements, and Dr. Roger Vincent (Department of Physics, University of Bristol) for performing the transmission electron microscopy.

References

Bai Q, Kohlstedt DL (1992) Substantial hydrogen solubility in olivine and implications for water storage in the mantle. Nature 357:672–674

Bai Q, Kohlstedt DL (1993) Effects of chemical environment on the solubility and incorporation mechanism for hydrogen in olivine. Phys Chem Miner 19:460–471

Bell DR, Rossman GR (1992) Water in Earth's mantle: the role of nominally anhydrous minerals. Science 255:1391–1397

Beran A, Putnis A (1983) A model of the OH positions in olivine, derived from infrared-spectroscopic investigations. Phys Chem Miner 9:57–60

Braithwaite JS, Wright K, Catlow CRA (2003) A theoretical study of the energetics and IR frequencies of hydroxyl defects in forsterite. J Geophys Res (in press)
Brodholt JP (1997) Ab initio calculations on point defects in forsterite (Mg_2SiO_4) and implications for diffusion and creep. Am Mineral 82:1049–1053
Brodholt JP, Refson K (2000) An ab initio study of hydrogen in forsterite and a possible mechanism for hydrolytic weakening. J Geophys Res 105:18977–18982
Franck S, Bounama C (1995) Effect of water-dependent creep rate on the volatile exchange between mantle and surface reservoirs. Phys Earth Planet Int 92:57–65
Freund F, Oberheuser G (1986) Water dissolved in olivine: a single-crystal infrared study. J Geophys Res 91:745–761
Hirose K, Kawamoto T (1995) Hydrous partial melting of lherzolite at 1 GPa—the effect of H_2O on the genesis of basaltic magmas. Earth Planet Sci Lett 133:463–473
Hirth G, Kohlstedt DL (1996) Water in the oceanic upper mantle: implications for rheology, melt extraction and evolution of the lithosphere. Earth Planet Sci Lett 144:93–108
Ingrin J, Skogby H (2000) Hydrogen in nominally anhydrous upper-mantle minerals: concentration levels and implications. Eur J Mineral 12:543–570
Jamtveit B, Brooker R, Brooks K, Larsen LM, Pedersen T (2001) The water content of olivines from the North Atlantic Volcanic Province. Earth Planet Sci Lett 186:401–415
Jung H, Karato S (2001) Water-induced fabric transitions in olivine. Science 293:1460–1463
Karato S (1990) The role of hydrogen in the electrical conductivity of the upper mantle. Nature 347:272–273
Karato S, Jung H (1998) Water, partial melting and the origin of the seismic low velocity and high attenuation zone in the upper mantle. Earth Planet Sci Lett 157:193–207
Kitamura M, Kondoh S, Morimoto, N, Miller GH, Rossman GR, Putnis A (1987) Planar OH-bearing defects in mantle olivine. Nature 328:143–145
Kohlstedt DL, Keppler H, Rubie DC (1996) Solubility of water in the a, b and g phases of $(Mg,Fe)_2SiO_4$. Contrib Mineral Petrol 123:345–357
Kohn SC (1996) Solubility of H_2O in nominally anhydrous mantle minerals using ^1H MAS NMR. Am Mineral 81:1523–1526
Kushiro I, Yoder HS (1969) Melting of forsterite and enstatite at high pressures under hydrous conditions. Carnegie Inst Wash Yearb 67:153–158
Libowitzky E (1999) Correlation of O-H stretching frequencies and O-H...O hydrogen bond lengths in minerals. Mh Chem 130:1047–1059
Libowitzky E, Beran A (1995) OH defects in forsterite. Phys Chem Miner 22:387–392
Libowitzky E, Rossman GR (1996) Principles of quantitative absorbance measurements in anisotropic crystals. Phys Chem Miner 23:319–327
Libowitzky E, Rossman GR (1997) An IR absorption calibration for water in minerals. Am Mineral 82:1111–1115
Mackwell S, Kohlstedt D (1990) Diffusion of hydrogen in olivine: implications for water in the mantle. J Geophys Res 95:5079–5088
Matveev S, O'Neill HStC, Ballhaus C, Taylor WR, Green DH (2001) Effect of silica activity on OH^- IR spectra of olivine: implications for low-$a$$SiO_2$ mantle metasomatism. J Petrol 42:721–729
Miller GH, Rossman GR, Harlow GE (1987) The natural occurrence of hydroxide in olivine. Phys Chem Miner 14:461–472
Redfern SAT, Artioli G, Rinaldi R, Henderson CMB, Knight KS, Wood BJ (2000) Octahedral cation ordering in olivine at high temperature. II: an in situ neutron powder diffraction study on synthetic $MgFeSiO_4$ (Fa50). Phys Chem Miner 27:630–637
Richard G, Monnereau M, Ingrin J (2002) Is the transition zone an empty water reservoir? Inferences from numerical model of mantle dynamics. Earth Planet Sci Lett 205:37–51
Rossman GR, Aines RD (1991) The hydrous components in garnet: grossular-hydrogrossular. Am Mineral 76:1153–1164
Sciuto PF, Ottonello G (1995) Water-rock interaction on Zabargad Island, Red Sea: a case study: I. Application of the concept of local equilibrium. Geochim Cosmochim Acta 59:2187–2206